Supplemental Data
for

Identification and Functional and Spectral Characterization of a Globin-coupled Histidine Kinase from *Anaeromyxobacter* sp. Fw109-5*

Kenichi Kitanishi[‡], Kazuo Kobayashi[§], Takeshi Uchida[¶], Koichiro Ishimori[¶], Jotaro Igarashi[‡], and Toru Shimizu[‡,1]

From the [‡]Institute of Multidisciplinary Research for Advanced Materials, Tohoku University, Katahira, Aoba-ku, Sendai 980-8577, Japan, the [§]Institute of Scientific and Industrial Research, Osaka University, Mihogaoka, Ibaraki, Osaka 567-0047, Japan and the [¶]Department of Chemistry, Faculty of Science, Hokkaido University, Sapporo 060-0810, Japan

Table S1. Oligonucleotides used for the construction of expression vectors for generating mutant proteins. The underlined bases indicate the introduced mutations.

Mutants	Primer sequences	
Anae109_2438		
Y45F [a]	5’-GAATTTTTCGATCGTATCCTGGGGCAT-3’	Forward
	5’-ACGATCGAAAAATTCCTCGGCCAGGCG-3’	Reverse
Y45L [a]	5’-GAATTTCTGGATCGTATCCTGGGGCAT-3’	Forward
	5’-ACGATCCAGAAATTCCTCGGCCAGGCG-3’	Reverse
Y45W [a]	5’-GAATTTTGGGATCGTATCCTGGGGCAT-3’	Forward
	5’-ACGATCCCAAAATTCCTCGGCCAGGCG-3’	Reverse
H99A [b]	5’-TTATCGTATTGGTCGTGTTGCCGTCCGTATCGGACTGC-3’	Forward
	5’-GCAGTCCGATACGGACGGCAACACGACCAATACGATAA-3’	Reverse
H183A [a]	5’-ATTGGAGCCGATCTGCGCAATCCTCTG-3’	Forward
	5’-CAGATCGGCTCCAATAGAACCGACCAG-3’	Reverse
Anae109_2439		
D52A [b]	5’-TGCCCTGCTGACAGCCATGCGTATGCCTC-3’	Forward
	5’-GAGGCATACGCATGGCTGTCAGCAGGGCA-3’	Reverse
D169A [a]	5’-CTGGTGGCTCTGCGTGTTCCTGGTGGT-3’	Forward
	5’-ACGCAGAGCCACCAGAGCACAAAAAGG-3’	Reverse

[a] Using the PrimeSTAR mutagenesis basal kit (Takara Bio)
[b] Using the QuikChange site-directed mutagenesis kit (Stratagene)

Table S2. Spin state and coordination marker bands of resonance Raman spectra of the Fe(III), Fe(II), Fe(II)-O_2 and Fe(II)-CO complexes of full-length wild-type and Y45F mutant *Af*GcHKs. The proposed coordination structures are described in the far-right hand column.

		ν_2	ν_3	ν_4	Coordination structure
WT	Fe(III)	1578	1502	1374	6cLS
	Fe(II)	1558	1470	1354	5cHS
	Fe(II)-O_2	1579	1501	1375	6cLS
	Fe(II)-CO	1581	1496	1372	6cLS
Y45F	Fe(III)	1577	1502	1374	6cLS
	Fe(II)	1558	1469	1354	5cHS
	Fe(II)-O_2	1579	1500	1375	6cLS
	Fe(II)-CO	1581	1495	1372	6cLS
					(cm^{-1})

6cLS, 6-coordinated low spin; 5cHS, 5-coordinated high spin

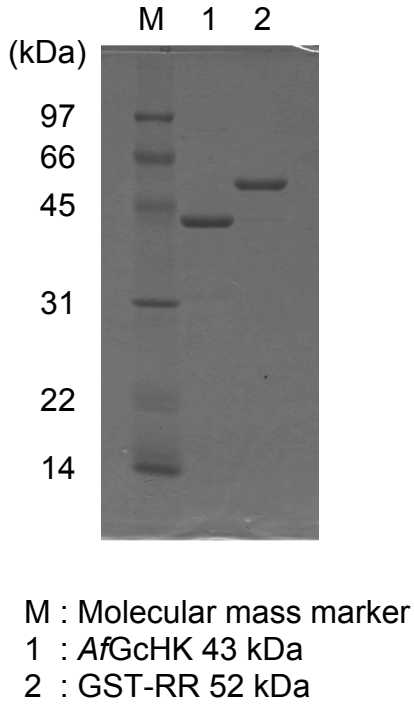

Fig. S1. SDS-PAGE demonstrating >90% homogeneity of purified full-length *Af*GcHK (lane 1) and GST-RR (lane 2).

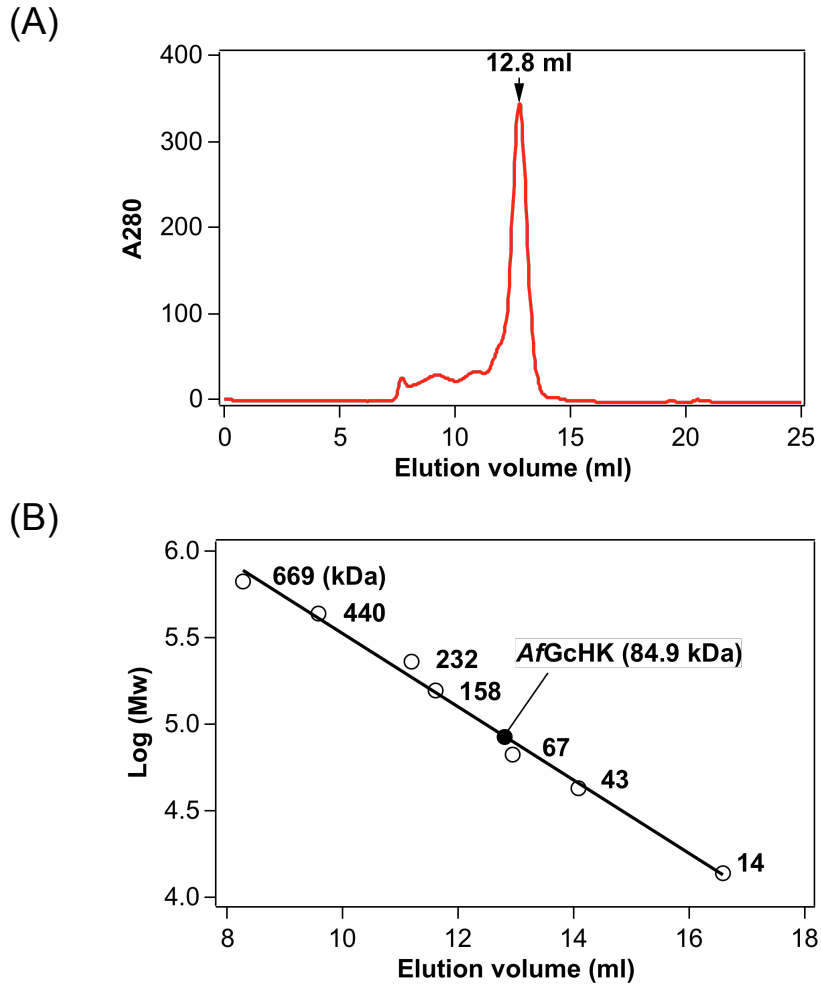

Fig. S2. Gel filtration chromatography pattern for *Af*GcHK. (A) Superdex 200 HR10/30 gel filtration column chromatography of full-length wild-type *Af*GcHK monitored at 280 nm. (B) Correlation between the elution volumes in gel filtration and estimated molecular weights of full-length wild-type *Af*GcHK. The molecular mass of *Af*GcHK was estimated as 84.9 kDa. The molecular mass predicted from the amino acid sequence was 43.0 kDa, suggesting that the purified protein is dimeric.

(A)

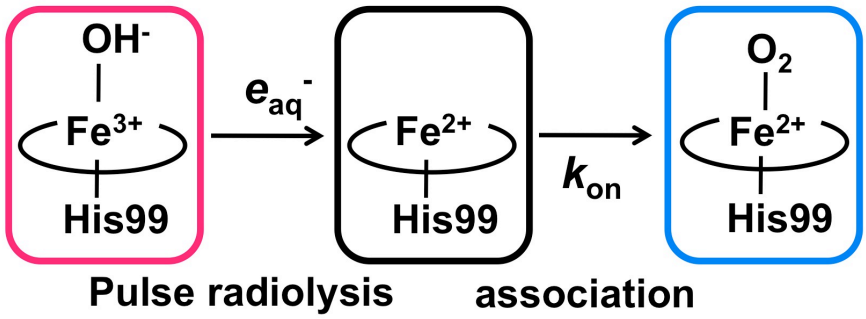

(B)

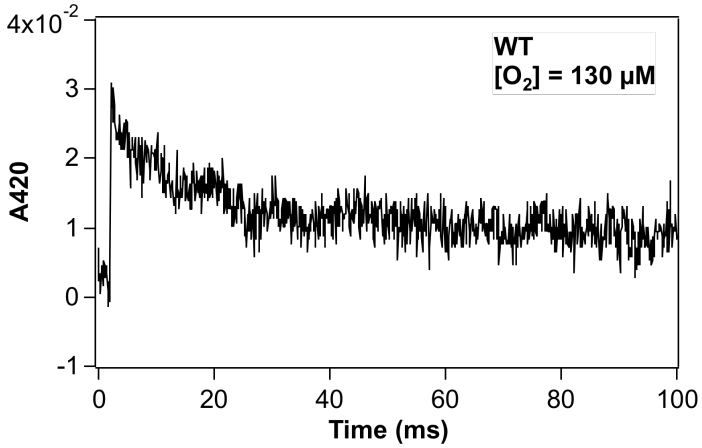

Fig. S3. (A) Coordination structural changes from the Fe(III) complex to the Fe(II)-O_2 complex via the Fe(II) complex induced by pulse radiolysis. (B) Spectral changes (monitored at 420 nm) accompanying association of O_2 to the Fe(II) complex (or conversion from the Fe(II) to Fe(II)-O_2 complex) of wild-type full-length *Af*GcHK, using pulse radiolysis. Protein concentration: 10 μM, buffer: 10 mM phosphate, pH 7.4 and 0.1 M *tert*-butyl alcohol.

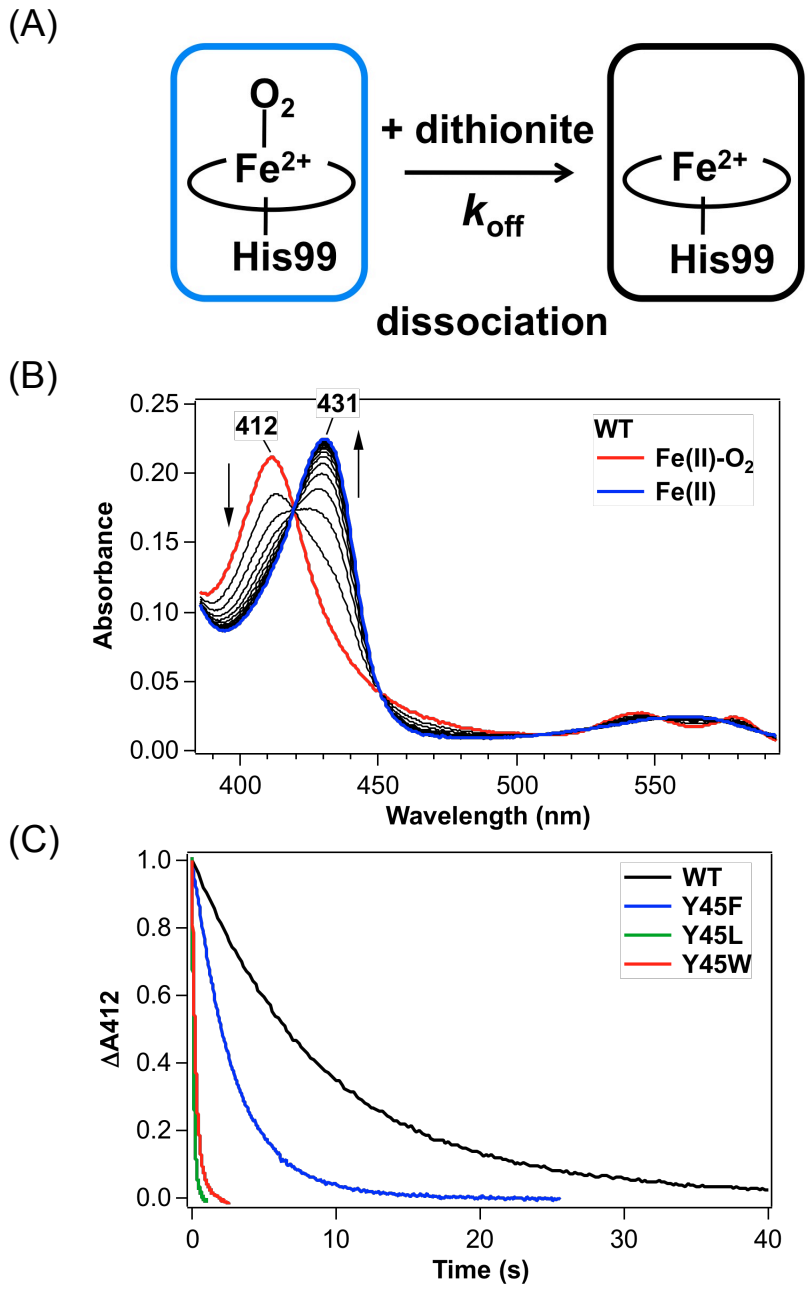

Fig. S4. (A) Coordination structural changes from the Fe(II)-O_2 complex to the Fe(II) complex with the addition of dithionite. (B) Spectral changes accompanying dissociation of O_2 from the Fe(II) complex (or conversion from the Fe(II)-O_2 to Fe(II) complex) of wild-type full-length *Af*GcHK. (C) Traces of spectral changes monitored at 412 nm for the wild-type, Y45F, Y45L and Y45W mutant proteins are presented. Protein concentration: 2 μM Fe(II)-O_2 complex, buffer: 50 mM Tris-HCl, pH 8.0.

(A)

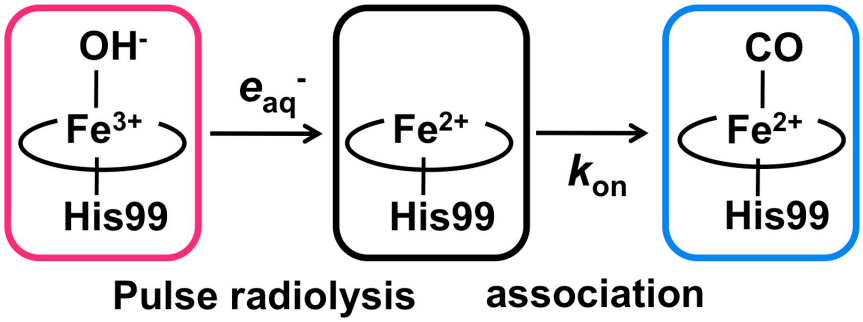

(B)

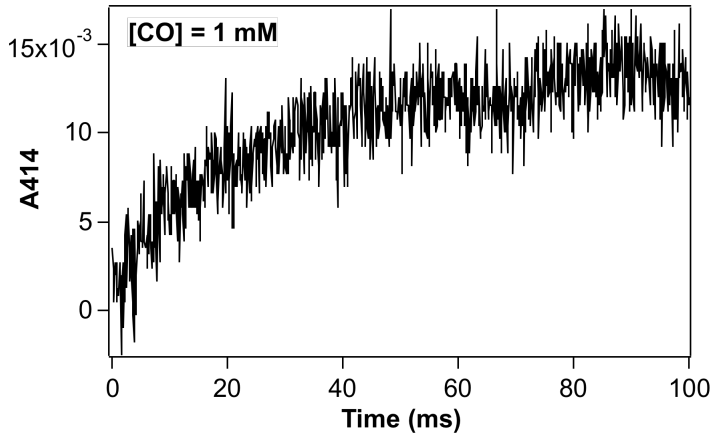

Fig. S5. (A) Coordination structural changes from the Fe(III) complex to the Fe(II)-CO complex via the Fe(II) complex induced by pulse radiolysis. (B) Spectral changes (monitored at 414 nm) accompanying association of CO with the Fe(II) complex (or conversion from the Fe(II) to Fe(II)-CO complexes) for wild-type full-length *Af*GcHK, using pulse radiolysis. Protein concentration: 10 μM, buffer: 10 mM phosphate, pH 7.4 and 0.1 M *tert*-butyl alcohol.

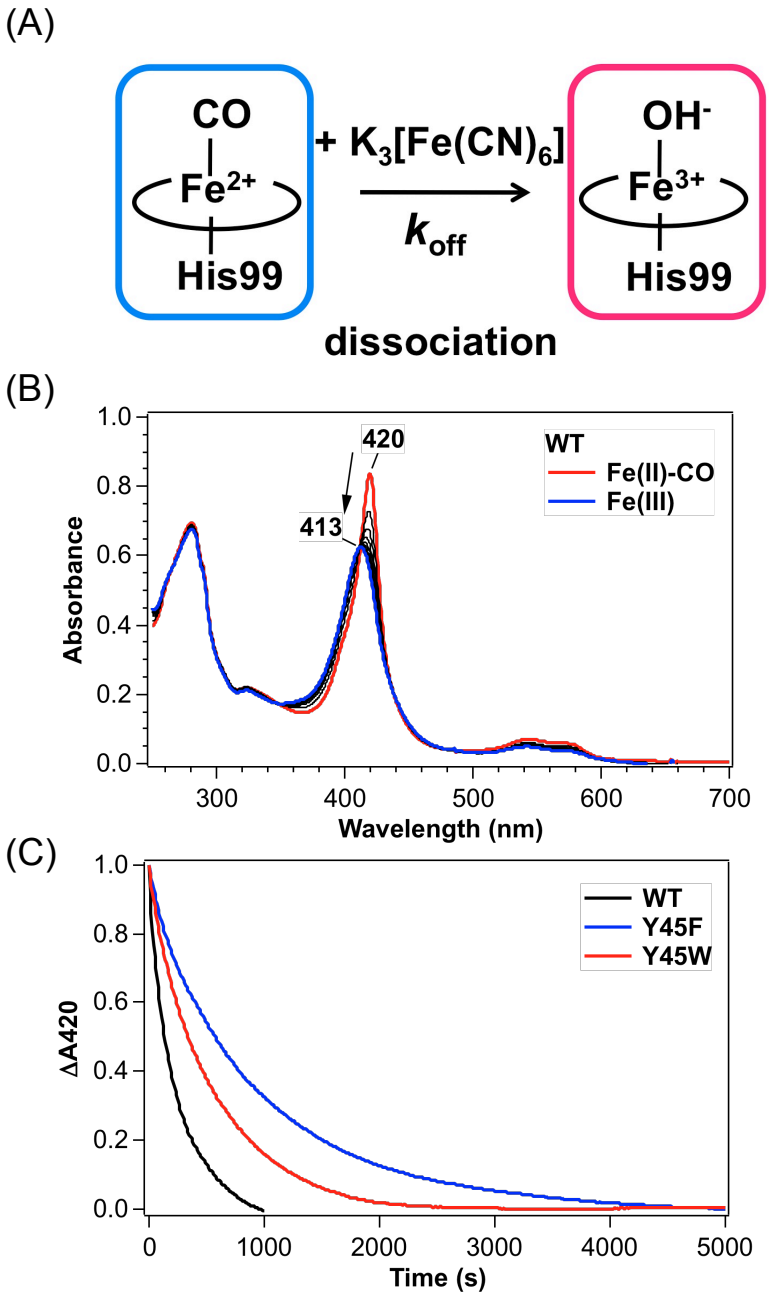

Fig. S6. (A) Coordination structural changes from the Fe(II)-CO to Fe(III) complex caused by adding ferricyanide. (B) Spectral changes accompanying dissociation of CO from the Fe(II) complex (or conversion from the Fe(II)-CO to Fe(III) complexes) of wild-type full-length *Af*GcHK. (C) Traces of spectral changes monitored at 420 nm for the wild-type, Y45F and Y45W mutant proteins are shown. Protein concentration: 5 μM Fe(II)-CO complex, buffer: 50 mM Tris-HCl, pH 8.0.

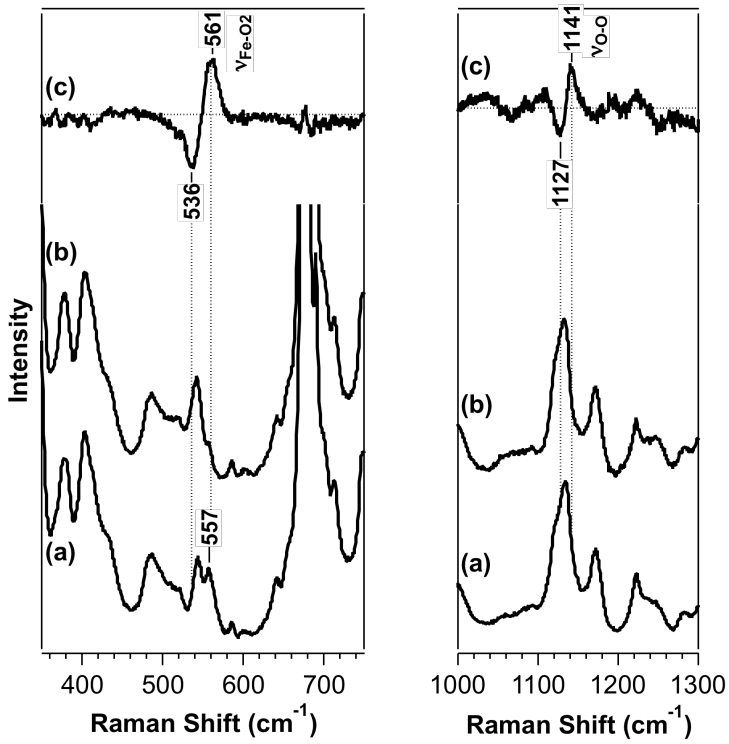

Fig. S7. Resonance Raman spectra of the Fe(II)-O_2 complex of wild-type, full-length *Af*GcHK in the low (left panel) and high frequency (right panel) regions, with excitation at 413.1 nm. Spectra of complexes with $^{16}O_2$ (a) and $^{18}O_2$ (b) and the difference spectrum ($^{16}O_2$ - $^{18}O_2$) (c) are depicted. See MATERIALS AND METHODS for experimental details.

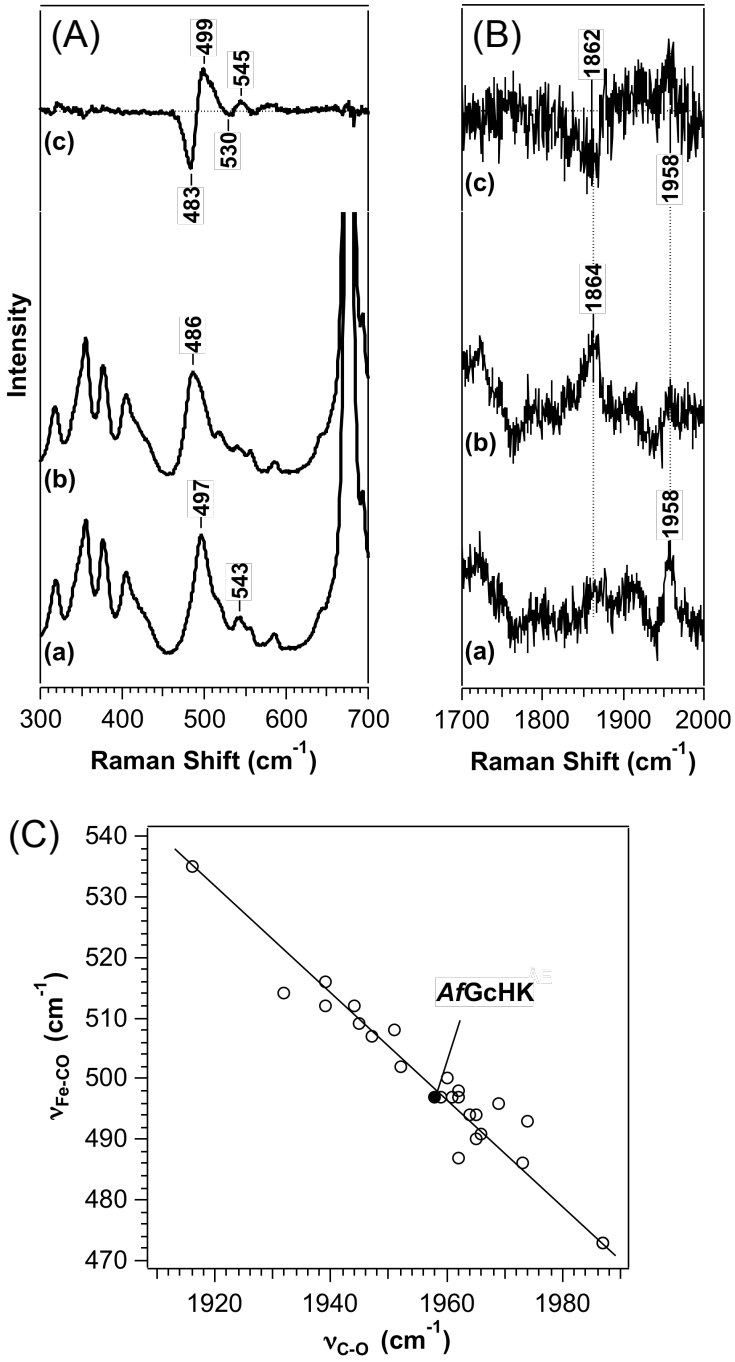

Fig. S8. Resonance Raman spectra of the Fe(II)-CO complex of full-length *Af*GcHK in the low (A) and high frequency (B) regions, with excitation at 413.1 nm. Spectra of protein complexes with $^{12}C^{16}O$ (a) and $^{13}C^{18}O$ (b) and their difference spectrum ($^{12}C^{16}O$ - $^{13}C^{18}O$) (c) are shown in (A) and (B). An inverse correlation plot between the $\nu_{Fe\text{-}CO}$ and $\nu_{C\text{-}O}$ frequencies of the Fe(II)-CO complex is presented (C). See MATERIALS AND METHODS for experimental details.

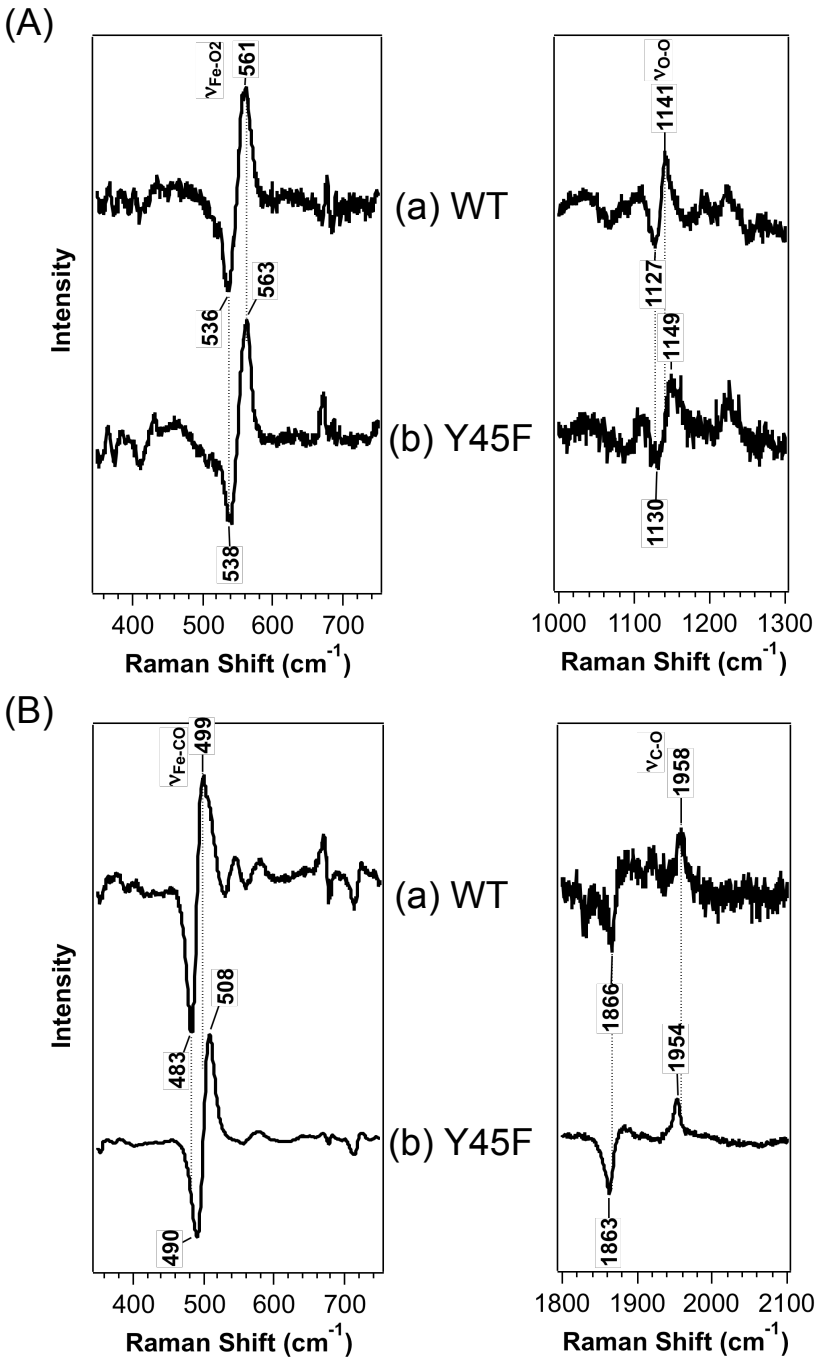

Fig. S9. (A) Difference resonance Raman spectra representing the differences ($^{16}O_2$ - $^{18}O_2$) in the Fe(II)-O_2 complexes of wild-type and Y45F full-length *Af*GcHK in the low (left panel) and high frequency (right panel) regions, with excitation at 413.1 nm. (B) Difference resonance Raman spectra representing differences ($^{12}C^{16}O$ - $^{13}C^{18}O$) in the Fe(II)-CO complexes of full-length wild-type and Y45F *Af*GcHKs in the low (left panel) and high frequency (right panel) regions, with excitation at 413.1 nm. (a) Wild-type and (b) Y45F proteins. Frequencies of the $\nu_{Fe\text{-}O2}$, $\nu_{O\text{-}O,}$ $\nu_{Fe\text{-}CO}$ and $\nu_{C\text{-}O}$ modes of the wild-type and mutant proteins are summarized in Table 4. See MATERIALS AND METHODS for experimental details.

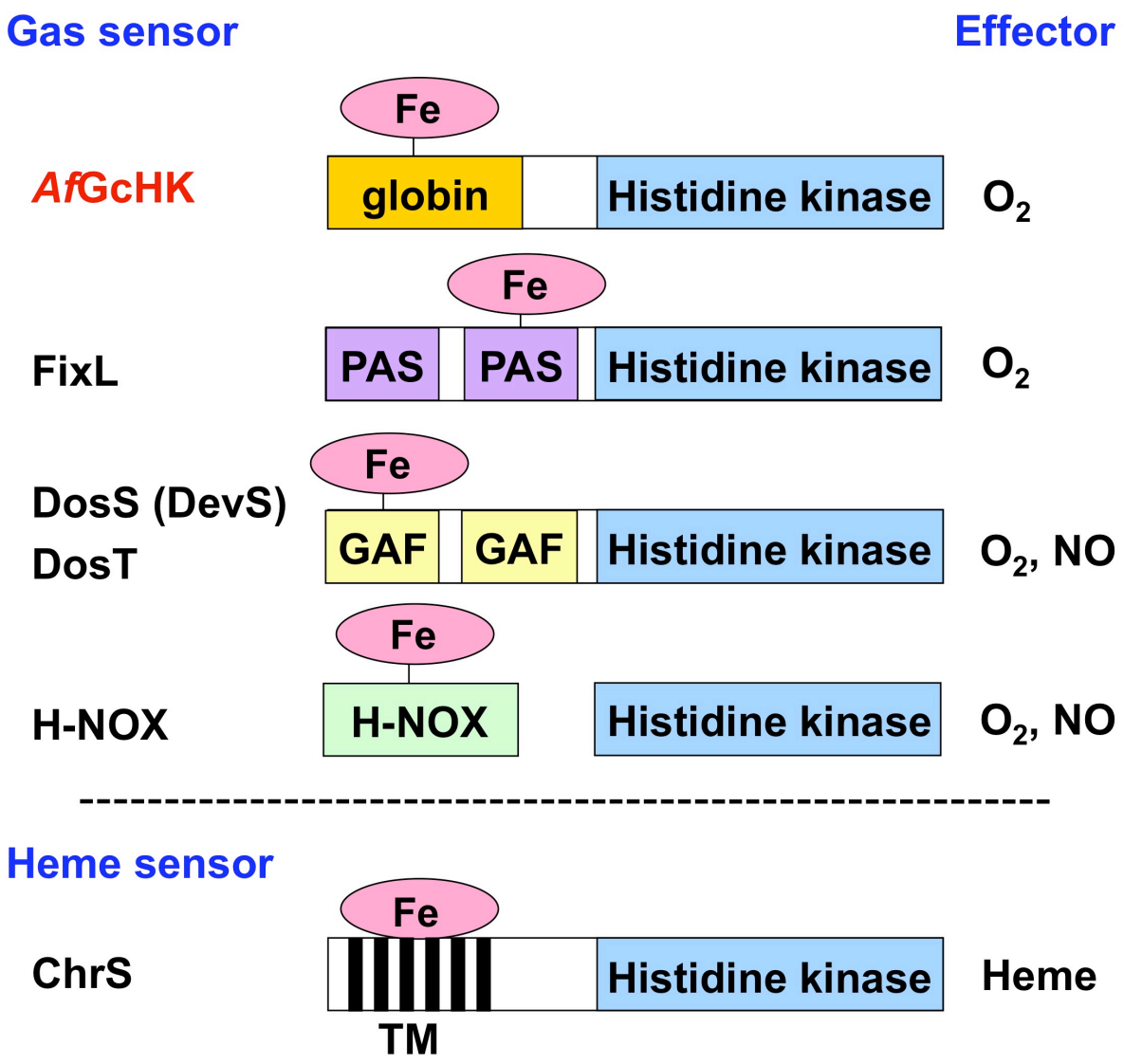

Fig. S10. Heme-regulated histidine kinases. For FixL, DosS (DevS), DosT, and H-NOX, the heme iron complex is bound to the PAS, GAF or H-NOX domain, and acts as the O_2 (or NO) binding (or sensing) site as the oxygen (or gas) sensor enzyme. *Af*GcHK, a novel histidine kinase with the heme iron complex bound within the globin domain (globin-coupled oxygen sensor), has been identified and characterized for the first time in this study. ChrS is a heme sensor histidine kinase in which association/dissociation of the heme iron complex to the transmembrane (TM) domain regulates histidine kinase function.